An Organelle-like Structure Correlated with the Quiescent State of Bacterial Cells

Jiayu Yu[1†], Yang Liu[1†] & Zengyi Chang[1,2,*]

[1]The State Key Laboratory of Protein and Plant Gene Research, School of Life Sciences, Peking University, Beijing 100871, P.R. China
[2]Center for Protein Science, Peking University, Beijing 100871, P.R. China
[†]J.Y. and Y.L. contributed equally to this work
[*]Correspondence: changzy@pku.edu.cn (Z.C.)

Abstract

The prokaryotic tubulin homolog protein FtsZ assembles into the Z-ring at mid-cell to provide contractile force during bacterial cell division. Here, by tracing the status of FtsZ in living *E. coli* cells, we unexpectedly revealed a cytosolic organelle-like structure containing the FtsZ protein that is solely formed in non-growing/non-dividing late stationary-phase cells and is located at the cell poles. This structure, which we named the quiescent body, contains selected essential proteins involved in cell growth and division, and its formation depends on the operation of the cellular respiratory chain. The quiescent bodies start to disassemble to release the important proteins that will resume functioning upon cell re-growth/re-division under permissive growth conditions, while those cells containing intact quiescent bodies do not re-grow/re-divide. Meanwhile, the quiescent bodies endow the cells with a higher antibiotic resistance capacity by inhibiting cell recovery. Our discoveries reported here strongly suggest that the quiescent bodies sequester proteins important for cell growth/division and thus maintain the cells in a quiescent state. These findings also implicate that bacterial pathogens might be effectively killed by antibiotics that only target growing cells by blocking the assembly or promoting the disassembly of quiescent bodies.

Cell division is an essential event for the propagation of all species. Bacterial cell division is known to occur by the formation of a divisome, a dynamic structure assembled from many different proteins, in the middle of the parent cell before its division into two daughter cells[1–3]. The FtsZ protein, a conserved tubulin-like GTPase that has been identified as the major component of the divisome, assembles into a ring-like structure called the Z-ring, which in turn recruits other proteins and provides the contractile force for bacterial cytokinesis[4,5]. Although it is known that the FtsZ protein subunits are able to form fibrous protofilaments via head-to-tail associations, little is

known about how these protofilaments further assemble into the Z-ring and how the Z-ring generates the contractile force to accomplish cell division[6–8].

We have been interested in understanding how the FtsZ protein assembles into the Z-ring structure by identifying its amino acid residues that mediate the assembly process in living *E. coli* cells. To this end, our major approach was to individually substitute selected amino acid residues in the FtsZ protein with the unnatural amino acid *p*-benzoyl-L-phenylalanine (pBpa), which could be activated upon exposure to UV light and allow FtsZ to form a covalent linkage with an interacting partner [9–13], either another FtsZ subunit (resulting in the formation of photocrosslinked FtsZ dimers) or other proteins. Such *in vivo* photocrosslinking experiments performed with dividing log-phase *E. coli* cells allowed us not only to validate previously reported amino acid residues but also to identify new residues that are involved in forming the Z-ring (data to be published elsewhere). Initially designed as a control experiment, we also performed a similar *in vivo* photocrosslinking analysis with non-growing/non-dividing late stationary-phase cells in which the Z-ring was assumed to be disassembled[5,6,14], and thus photocrosslinked FtsZ dimer products were not expected to form. Strikingly, we still detected photocrosslinked products, not only as FtsZ-FtsZ dimers but also as complexes between FtsZ and other proteins, when pBpa was introduced at certain residue positions of FtsZ (data to be reported later). These observations, although unexpected, strongly indicate that the FtsZ protein is not randomly dispersed in the cytosol in late stationary-phase cells, and they prompted us to conduct an extensive study on the status of the FtsZ protein in these cells, with the striking results being reported here.

In this study, by tracing the status of the FtsZ protein, we unexpectedly revealed a unique cytosolic organelle-like structure that is formed in the non-growing/non-dividing late stationary-phase *E. coli* cells. This structure, which we named the quiescent body, is located at the cell poles and contains selected important proteins involved in cell (re)-growth and (re)-division. The disassembly of quiescent body upon cell re-growth/re-division for releasing the sequestered proteins that will resume their function is rather heterogeneous among different individual cells, and those cells containing intact quiescent bodies fail to regrow under permissive growth conditions. Our findings reported here strongly suggest that specifically selected proteins are sequestered in the quiescent body so that make the cell entry into a quiescent state which endows the cell with antibiotic resistance capacity. Our discoveries also imply that blocking the assembly or promoting the disassembly of quiescent bodies would likely put bacterial pathogens into an actively growing state, enabling them to be killed by antibiotics.

Results

FtsZ protein was found to exist as cell pole granules in non-growing/non-dividing late stationary-phase cells and to re-assemble into a Z-ring upon cell re-growth/re-division

To gain insight into the status of the FtsZ protein in bacterial cells at different growth/division states, we heterologously expressed the fluorescent protein mNeonGreen-fused FtsZ at a low level that FtsZ-mNeonGreen will label but not disrupt the structure formed by the endogenous wild-type FtsZ, and thus allow the structure to be visualized by live-cell imaging[15]. The Z-ring was clearly visualized in the middle of growing/dividing log-phase cells (**Fig. 1a** top panel). Strikingly, when we analyzed the non-growing/non-dividing late stationary-phase cells, we observed that the FtsZ proteins were localized at the cell poles in the form of granules (**Fig. 1a** bottom panel). As a control, the mNeonGreen protein (not fused to FtsZ) was observed to evenly spread in the cytosol of either log-phase or late stationary-phase cells (**Supplementary Fig. 1A**). Collectively, these results indicate that the FtsZ proteins exist as cell pole granules in late stationary-phase cells.

We next analyzed the fate of the FtsZ proteins in the cell pole granules upon cell re-growth and re-division. For this purpose, we constructed a new strain by inserting the gene encoding the FtsZ-mNeonGreen fusion protein into the genomic rhamnose operon so that its expression is controlled by rhamnose (**Supplementary Fig. 1B**). We verified that the expression of FtsZ-mNeonGreen in this strain depended on the induction of rhamnose (**Supplementary Fig. 1C**), and the cell growth rates were indistinguishable in the presence or absence of rhamnose (**Supplementary Fig. 1D**). With this *ftsZ-mNeonGreen* strain, we also observed the Z-ring structure and cell pole granules in log-phase and late stationary-phase cells, respectively, under fluorescence microscopy (**Supplementary Fig. 1E**).

Then late stationary-phase *ftsZ-mNeonGreen* cells were re-cultured in rhamnose-lacking fresh media (thus no new FtsZ-mNeonGreen protein would be synthesized). The live-cell imaging data presented in **Fig. 1b** reveal a remarkable time-dependent disappearance of the FtsZ-mNeonGreen proteins present in the cell pole granules and the subsequent appearance of the protein in the newly formed Z-ring only for those cells that started to re-grow/re-divide (as indicated by the white dashed circles). These observations indicate that the FtsZ proteins in cell pole granules re-assemble into a Z-ring upon cell re-growth/re-division. Notably, those cells containing intact cell pole granules did not re-grow/re-divide (as indicated by the red dashed circles) (**Fig. 1b**), indicating that the disassembly of the cell pole granules is highly asynchronous for different individual cells, which apparently corresponds to the great diversity in the recovery time for individual late stationary-phase cells, as reported previously [16–18].

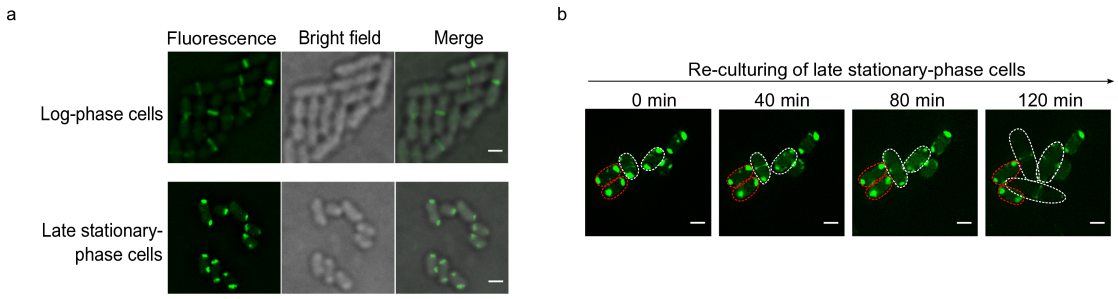

Figure 1. Live-cell fluorescence microscopy imaging reveals that the FtsZ-mNeonGreen protein is present in cell pole granules in late stationary-phase *E. coli* cells and re-assembles into a newly formed Z-ring upon cell re-growth/re-division.
(a) Fluorescence and bright field images of the log-phase (6 h; top panel) and late stationary-phase (24 h; bottom panel) cells in which the FtsZ-mNeonGreen protein was heterologously expressed in addition to the endogenous wild-type FtsZ. **(b)** Fluorescence images of the late stationary-phase *ftsZ-mNeonGreen* cells (with the gene encoding the FtsZ-mNeonGreen protein integrated into the genomic rhamnose operon, as illustrated in **Supplementary Fig. 1B**) that were re-cultured at 37℃ to the indicated time points in rhamnose-lacking fresh LB media. The re-growing and non-growing cells are indicated by white and red dashed lines, respectively. Scale bars, 1 μm.

The cell pole granules possess a compact organelle-like structure in which almost all the FtsZ proteins in late stationary-phase cells are located

To clarify the exact sub-cellular localization of the cell pole granules, we separately labeled the cytosol, the inner membrane and the outer membrane with the red fluorescent protein mCherry, inner membrane anchoring peptide (derived from the nlpA protein)-fused mCherry and outer membrane protein A (OmpA)-fused mCherry in *ftsZ-mNeonGreen* cells, respectively. The live-cell imaging data displayed in **Fig. 2a** clearly demonstrate that each cell pole granule occupies a cytosolic space that is completely inaccessible to the cytosolic mCherry proteins and thus represents a compact organelle-like structure.

We subsequently attempted to examine whether such cell pole granules can be released as intact structures when the cells are disrupted. For this purpose, we first prepared late stationary-phase *ftsZ-mNeonGreen* cells in rhamnose-containing media and then lysed the cells (with a French press) before visualizing the cell lysates with fluorescence microscopy. The micrographs displayed in **Fig. 2b** show that the cell pole granules remain as intact entities even in the lysates. Additionally, we found that such entities could be effectively collected in the pellet when the cell lysates were subjected to centrifugation (data not shown).

To examine the proportion of the cellular FtsZ proteins located in the cell pole granules, we then analyzed the supernatant and pellet fractions of the lysates of the late stationary-phase *ftsZ-mNeonGreen* cells by immunoblotting analysis. The results, as displayed in **Fig. 2c**, clearly show that both the wild-type and mNeonGreen-fused FtsZ proteins are largely detected in the pellet fraction (lane 6) while hardly any were

154 detected in the supernatant fraction (lane 5). In contrast, for the log-phase cells (in
155 which no cell pole granules are formed), both the wild-type and fused FtsZ proteins
156 were largely detected in the supernatant fraction (**Fig. 3c**, lane 2). We also observed
157 similar patterns of FtsZ distribution in the wild-type cells (**Fig. 2d**), indicating that total
158 FtsZ proteins indeed occur as cell pole granules in late stationary-phase wild-type cells.
159 Importantly, in contrast to the FtsZ protein, in the pellet fraction of the late
160 stationary-phase cells, we hardly detected any of GroEL protein, a member of the
161 Hsp60 family of molecular chaperones that is commonly found in such protein
162 aggregates as the inclusion bodies formed in bacteria[19], or of EF-Tu, one of the most
163 abundant proteins in the cytosol of *E. coli* cells (**Fig. 2d**). Taken together, these
164 observations strongly indicate that the cell pole granule represents an organelle-like
165 structure rather than a non-specific protein aggregate. Additionally, immunoblotting
166 analysis also indicated the presence of outer membrane components (as represented by
167 OmpF) in the pellet fraction, consistent with what has been reported before[20], but the
168 absence of inner membrane components (as represented by the α-subunit of ATP
169 synthase) (also shown in **Fig. 2d**).
170 We next examined whether the endogenous wild-type FtsZ in the cell pole granules
171 can be released to form the Z-ring structure when the late stationary-phase cells re-
172 grow/re-divide. To this end, the late stationary-phase *ftsZ-mNeonGreen* cells were re-
173 cultured in fresh media with protein synthesis (including that of FtsZ) inhibited by the
174 presence of chloramphenicol[21]. In this case, we observed a similar time-dependent
175 disappearance of the FtsZ-mNeonGreen proteins in the cell pole granules, accompanied
176 by the re-formation of the Z-ring structure (mainly relying on the wild-type FtsZ protein)
177 labeled by FtsZ-mNeonGreen (**Fig. 2e**). The data displayed in **Fig. 1b** and **Fig. 2e**
178 collectively indicate that the FtsZ proteins stored in the cell pole granules can be
179 released and re-assembled to form the Z-ring structure independent of new protein
180 synthesis when the late stationary-phase cells are placed in an environment permissive
181 to cell growth. In addition, the data presented in **Fig. 2e** once again indicate the
182 heterogeneity of cell pole granule disassembly among different individual cells.
183
184 **The cell pole granules contain functionally important proteins involved in cell**
185 **(re-)growth and (re-)division**
186
187 Given that the visualization of cell pole granules in the cell lysate under bright
188 field microscope (**Fig. 2b**) and the limited molecular number of FtsZ proteins in each
189 cell, other proteins are most likely also present in such granules. To identify these other
190 proteins, the cell pole granules collected in the pellets of cell lysates were dissolved in
191 8 M urea, concentrated and resolved by SDS-PAGE before the selected protein bands
192 that could be visualized on the gel (**Fig. 2f**, lane 10) were cut out and subjected to mass
193 spectrometric analysis. As listed in **Fig. 2g**, in addition to FtsZ, we also identified key
194 proteins involved in such fundamental biological processes as transcription (subunits

195 of RNA polymerase), translation (ribosomal proteins and aminoacyl tRNA synthetases),
196 metabolism and cell division.
197 Among the cell division proteins we identified in the cell pole granules (FtsZ,
198 FtsA, FtsE, FtsX, ZapC, MinD and MinE), we verified that FtsA and ZapC, although
199 located in the Z-ring structure in log-phase cells[15,22], are indeed present in the cell pole
200 granules in late stationary-phase cells (**Supplementary Fig. 2A**). Furthermore, FtsA
201 (tagged with mCherry) co-localizes with FtsZ (tagged with mNeonGreen) both in the
202 Z-ring of log-phase cells and in the cell pole granules of late stationary-phase cells or
203 the cell lysates, as shown in **Supplementary Fig. 2B**. As a control, the FtsL and ZapA
204 proteins, which were not identified in our mass spectrometric analysis but are known[23]
205 and confirmed by us to be present in the Z-ring in log-phase cells, were not detected in
206 the cell pole granules (**Supplementary Fig. 2A**). Taken together, our data (displayed
207 in **Fig. 2f** and **Supplementary Fig. 2**) apparently suggest that specific proteins essential
208 for cell (re)-growth and (re)-division are selectively sequestered in the cell pole
209 granules in late stationary-phase cells.
210

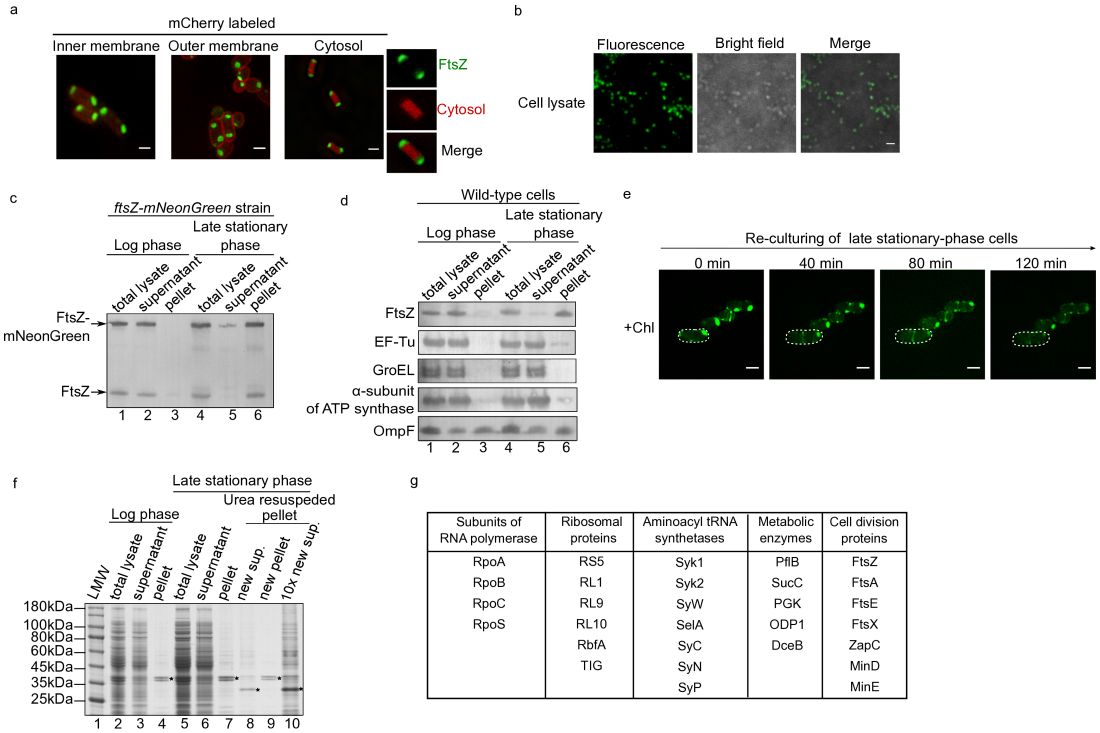

Subunits of RNA polymerase	Ribosomal proteins	Aminoacyl tRNA synthetases	Metabolic enzymes	Cell division proteins
RpoA	RS5	Syk1	PflB	FtsZ
RpoB	RL1	Syk2	SucC	FtsA
RpoC	RL9	SyW	PGK	FtsE
RpoS	RL10	SelA	ODP1	FtsX
	RbfA	SyC	DceB	ZapC
	TIG	SyN		MinD
		SyP		MinE

211
212 **Figure 2. The cell pole granules possess a compact organelle-like structure in the cytosol and**
213 **contain almost all the FtsZ protein as well as other functionally important proteins involved**
214 **in cell (re-)growth/(re-)division.**
215 **(a)** Separate and merged fluorescence images of late stationary-phase *ftsZ-mNeonGreen* cells
216 whose inner membrane, outer membrane or cytosol was labeled by the red fluorescent protein
217 mCherry. **(b)** Fluorescence and bright field images of the cell lysate of late stationary-phase *ftsZ-*
218 *mNeonGreen* cells. Scale bars, 1 μm. **(c)** Immunoblotting results for the total cell lysate (lanes 1
219 and 4), the supernatant (lanes 2 and 5) and the pellet (lanes 3 and 6) of log-phase and late
220 stationary-phase *ftsZ-mNeonGreen* cells, probed with antibody against FtsZ. Positions of the

221 protein bands for FtsZ and FtsZ-mNeonGreen are indicated on the left. **(d)** Immunoblotting results
222 for the total cell lysate (lanes 1 and 4), the supernatant (lanes 2 and 5) and the pellet (lanes 3 and
223 6) of log-phase and late stationary-phase wild-type *E. coli* cells, probed with antibodies against the
224 indicated proteins (i.e., FtsZ, EF-Tu, GroEL, α-subunit of ATP synthase or OmpF). **(e)**
225 Fluorescence images of late stationary-phase *ftsZ-mNeonGreen* cells that were re-cultured at 37℃
226 to the indicated time points in rhamnose-lacking fresh media in the presence of the antibiotic
227 chloramphenicol (which inhibits the synthesis of all proteins). The cell in which the cell pole
228 granules disappeared and a new Z-ring structure formed is indicated by the white dashed line.
229 Scale bars, 1 μm. **(f)** Results of SDS-PAGE analysis on the proteins present in the total lysate
230 (lanes 2 and 5), the supernatant (lanes 3 and 6) and the pellet (lanes 4 and 7) of the log-phase and
231 late stationary-phase cells, as visualized by Coomassie Blue staining. The pellet of the lysate (lane
232 7) for the late stationary-phase cells was dissolved in 8 M urea, and the new supernatant (new
233 sup.; lane 8) was further concentrated by approximately 10-fold before further analysis (lane 10).
234 Asterisks (in lanes 4 and 7-10) indicate bands identified by mass spectrometry as outer membrane
235 proteins OmpA, OmpF or OmpC, which were collected in the pellet fraction, likely as outer
236 membrane debris. **(g)** List of major proteins in the cell pole granule as identified by mass
237 spectrometry analysis.
238
239 **Formation of cell pole granules is highly asynchronous for different individual**
240 **cells, and indole is an effective but non-essential inducing factor**
241
242 We next attempted to identify the factors that induce the formation of cell pole
243 granules. We started by tracing the status of the FtsZ proteins in *E. coli* cells from log-
244 phase (6-h cultures) to late stationary-phase (24-h cultures) by performing live-cell
245 imaging at 3-h intervals. The data displayed in **Fig. 3a** demonstrate the following. First,
246 the Z-ring structure disassembled in some of the cells when cultured for 12 h. Second,
247 the cell pole granule began to appear (indicated by the white arrow) in some cells while
248 others still contained the Z-ring (indicated by the red arrow) when cultured for 15 h.
249 Third, the cytosolic FtsZ protein gradually assembled into the cell pole granules in more
250 and more cells from 18 h culturing. These observations suggest that the formation of
251 cell pole granules is asynchronous for different cells. We then tested whether the culture
252 media of late stationary-phase (24-h cultures) cells is able to induce the formation of
253 cell pole granules in actively dividing log-phase cells (6-h cultures). The data presented
254 in **Fig. 3b** demonstrate that the formation of cell pole granules is significantly
255 accelerated when the log-phase cells are placed in late stationary-phase culture media,
256 and they are fully formed in all cells at approximately 10 h (i.e., at the +4 h time point)
257 instead of at 21 h, as occurred under non-inducing conditions (**Fig. 3a**).
258 It is known that the amino acids are utilized as fuel molecules because of lacking
259 carbohydrates when cells enter into the stationary phase, producing ammonia as a
260 result[14,24]. In view of this knowledge, we tested whether ammonia is an inducing factor
261 for cell pole granule formation by examining both its time-dependent and dosage-
262 dependent effects. However, the formation of cell pole granules was not observed, even

263 though the Z-ring structure was no longer observable (e.g., 50 mM ammonia, +1 h) in
264 the treated log-phase cells (**Supplementary Fig. 3A**).
265 We then tested whether indole, a molecule that is known to accumulate in
266 stationary-phase culture media and is believed to act as an intercellular signal affecting
267 multiple physiological processes in cells[25,26], is an inducing factor. In this regard, our
268 experiments on time- and dosage-dependent effects demonstrate that cell pole granules
269 could effectively form in log-phase cells when treated with 5 mM indole for as short as
270 1 h, as revealed both by live-cell imaging (**Supplementary Fig. 3B**; **Fig. 3c**) and by
271 immunoblotting (**Fig. 3d**) analyses.
272 To gain insight into whether indole is an essential factor for inducing the formation
273 of cell pole granules, we deleted the *tnaA* gene encoding the tryptophanase enzyme,
274 which is responsible for converting L-tryptophan into indole[27]. We observed that cell
275 pole granules are still effectively formed in the late stationary-phase Δ*tnaA* cells
276 (**Supplementary Fig. 3C**), indicating that indole is an effective but not essential factor
277 for inducing the formation of cell pole granules.

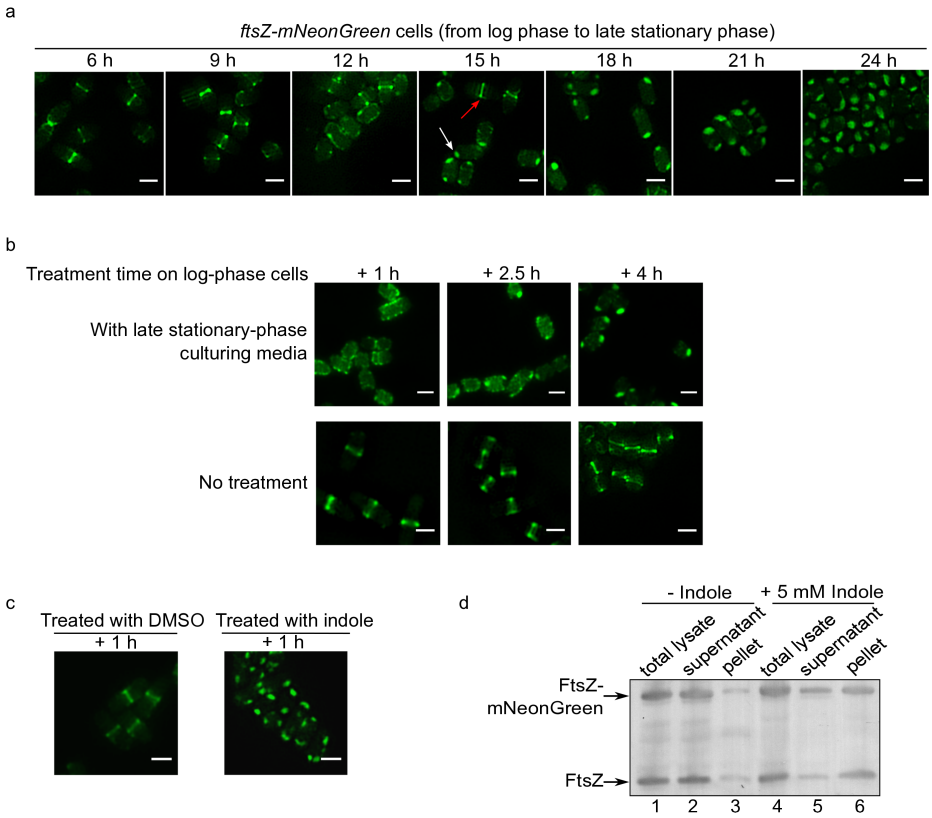

278
279 **Figure 3. Formation of cell pole granules is asynchronous in different individual cells, and**
280 **indole is able to accelerate their formation.**
281 **(a)** Fluorescence images recorded at the indicated time points for *ftsZ-mNeonGreen* cells cultured
282 in LB media containing 0.02% rhamnose. **(b)** Fluorescence images of log-phase *ftsZ-mNeonGreen*
283 cells, untreated (bottom panel) or treated with the late stationary-phase culture media for the
284 indicated length of time (top panel). **(c)** Fluorescence images of log phase *ftsZ-mNeonGreen* cells
285 treated with DMSO (the solvent used for dissolving indole) or indole (5 mM) for 1 h. Scale bars,
286 1 μm. **(d)** Immunoblotting results of the total cell lysate (lanes 1 and 4), the supernatant (lanes 2

287 and 5) and the pellet (lanes 3 and 6) of the log-phase *ftsZ-mNeonGreen* cells, untreated or treated
288 with indole (5 mM) for 1 h, probed with antibody against FtsZ. The positions of the protein bands
289 for FtsZ-mNeonGreen and FtsZ are indicated on the left.
290
291 **Formation of cell pole granules relies on the normal operation of the respiratory**
292 **chain**
293
294 In examining the induction effect of indole on cell pole granule formation, we
295 happened to observe that indole fails to induce cell pole granule formation in the
296 absence of oxygen (i.e., when the bacterial cells were cultured without shaking). Given
297 that indole is known to dissipate the proton gradient across the inner membrane of *E.*
298 *coli* cells, its induction effect might result from the acceleration of the electron transfer
299 process through the respiratory chain, which relies on the presence of oxygen[28]. In view
300 of this, we then addressed whether the induction effect of indole would be eliminated
301 when cellular respiration was inhibited. To this end, we added glucose, whose
302 metabolism is known to inhibit cellular respiration[24,29], to the culture media of log-
303 phase cells before treatment with indole in the presence of oxygen. In this case, we no
304 longer observed the formation of cell pole granules (**Fig. 4a**).
305 We next investigated whether cellular respiration is essential for the formation of
306 cell pole granules. For this purpose, we performed separate knockdown studies on the
307 *nuoA* and *sdhC* genes, which encode the NADH:ubiquinone oxidoreductase subunit A
308 of complex I and the succinate dehydrogenase subunit C of complex II (both
309 components of the respiratory chain), respectively, using CRISPRi technology[30]. The
310 live-cell imaging data presented in **Fig. 4b** and **Supplementary Fig. 4** demonstrate the
311 following. First, when either the *nuoA* gene or the *sdhC* gene was knocked down, cell
312 pole granules no longer formed in the log-phase cells that were treated with indole (**Fig**
313 **4b**). Second, formation of cell pole granules in late stationary-phase cells became
314 unobservable upon *sdhC* knockdown (**Fig. 4b**) or *sdhCDAB* (encoding all four subunits
315 of complex II) deletion (**Supplementary Fig. 4B**) and became significantly reduced
316 upon *nuoA* knockdown (**Fig. 4b**) or *nuoAB* (encoding two subunits of complex I)
317 deletion. Collectively, these observations indicate that the normal operation of the
318 respiratory chain is critical for the formation of cell pole granules.

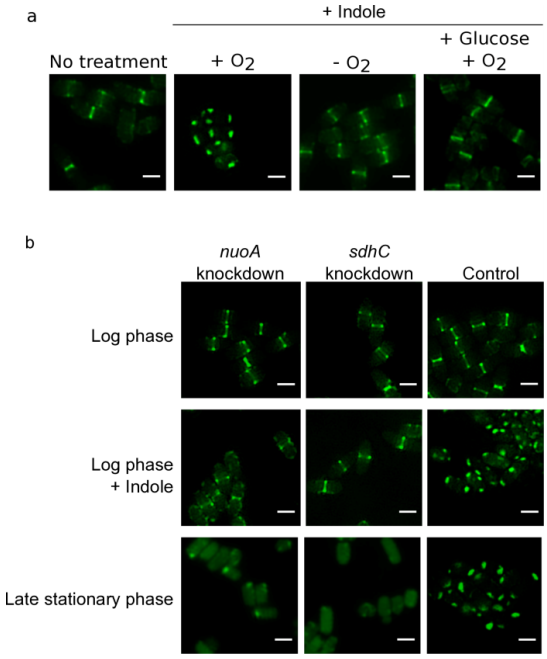

Figure 4. Normal operation of the respiratory chain is essential for the formation of cell pole granules

(a) Fluorescence images of log-phase *ftsZ-mNeonGreen* cells treated with indole (5 mM) for 1 h in the presence (+ O_2) or absence (- O_2) of oxygen or in the presence of both oxygen and glucose (0.2%) (+ Glucose, + O_2). **(b)** Fluorescence images of log-phase or late stationary-phase *ftsZ-mNeonGreen* cells with or without (as a control) the knockdown of the indicated genes and with the indicated indole treatment (5 mM, 1 h). Scale bars, 1 μm.

Formation of cell pole granules delays the re-growth/re-division process and endows the cell with a higher antibiotic resistance capacity

In our live-cell imaging studies on the re-cultured late stationary-phase cells described above (**Fig. 1b** and **Fig. 2e**), we also noticed that cell re-growth/re-division occurs only with the disappearance of the cell pole granules. This observation prompted us to perform a systematic analysis on the recovery processes for all the different types of cells we examined above, as reflected by their average initial doubling time upon re-division (T_{id}).

The values of the average initial doubling time upon re-division (T_{id}), calculated based on the re-culturing growth curves (**Supplementary Fig. 5**), demonstrate that the re-growth of cells in which cell pole granules have been formed is significantly delayed (**Fig. 5a** and **Fig. 5c**). In particular, first, the T_{id} of the indole-induced cell pole granule-containing log-phase wild-type cells is 67 min, approximately 2-fold longer than the 34 min of non-induced cell pole granule-lacking cells (**Fig. 5c**). Second, the T_{id} of the cell pole granule-containing stationary-phase wild-type cells is 100 min, approximately 3-fold longer than the 34 min of the cell pole granule-lacking log-phase cells (**Fig. 5c**). Third, the T_{id} of the stationary-phase *nuoA* knockdown cells containing a reduced level

347 of cell pole granules is 81 min, approximately 1.5-fold longer than the 48 min of the
348 cell pole granule-lacking log-phase *nuoA* knockdown cells (**Fig. 5c**). Fourth, the T_{id} of
349 the cell pole granule-lacking stationary-phase *sdhC* knockdown cells was largely
350 comparable with the cell pole granule-lacking log-phase *sdhC* knockdown or wild-type
351 cells, all approximately 35 min (**Fig. 5c**). Taken together, these observations strongly
352 suggest that functionally important proteins are somehow "locked" in the cell pole
353 granules such that the cells will not re-grow/re-divide until the proteins are released and
354 resume functioning.

355 The delayed recovery of the cell pole granule-containing bacterial cells would most
356 likely endow them with a higher capacity to resist antibiotics, given that only actively
357 growing/dividing cells can be effectively killed[31–33]. This assumption is confirmed by
358 a comparison of the survival rates, as presented in **Fig. 5b** and **Fig. 5d**, for these
359 different types of cells after being treated with two antibiotics, ofloxacin or ampicillin.
360 In particular, the results demonstrate that the survival rate of the indole-induced cell
361 pole granule-containing log-phase wild-type cells was approximately 10-fold higher
362 than that of the non-induced cell pole granule-lacking cells (**Fig. 5b**). In contrast, the
363 survival rate of the cell pole granule-lacking stationary-phase *sdhC* knockdown cells
364 was approximately 50-fold lower than that of cell pole granule-containing stationary-
365 phase wild-type cells, as similarly observed for the *nuoA* knockdown cells, although to
366 a lesser degree of approximately 5-fold (**Fig. 5d**). Taken together, these observations
367 indicate that the formation of the cell pole granules marks the entry into a quiescent
368 state that confers antibiotic resistance upon the bacterial cells. This correlation was also
369 directly observed by us with the *ftsZ-mNeonGreen* cells under fluorescence and bright
370 field microscopy, as shown by the data in **Fig. 5e**. Specifically, we observed that during
371 the recovery of the late stationary-phase cells in fresh media, only those that are re-
372 growing, as marked by a disappearance of their cell pole granules, will swell and die in
373 the presence of ampicillin (e.g., the cell indicated by the white dashed circles becomes
374 invisible). However, those that have not yet re-grown will survive (e.g., the cell
375 indicated by the red dashed circles maintained its cell pole granules and survived for
376 the whole period of examination).

377

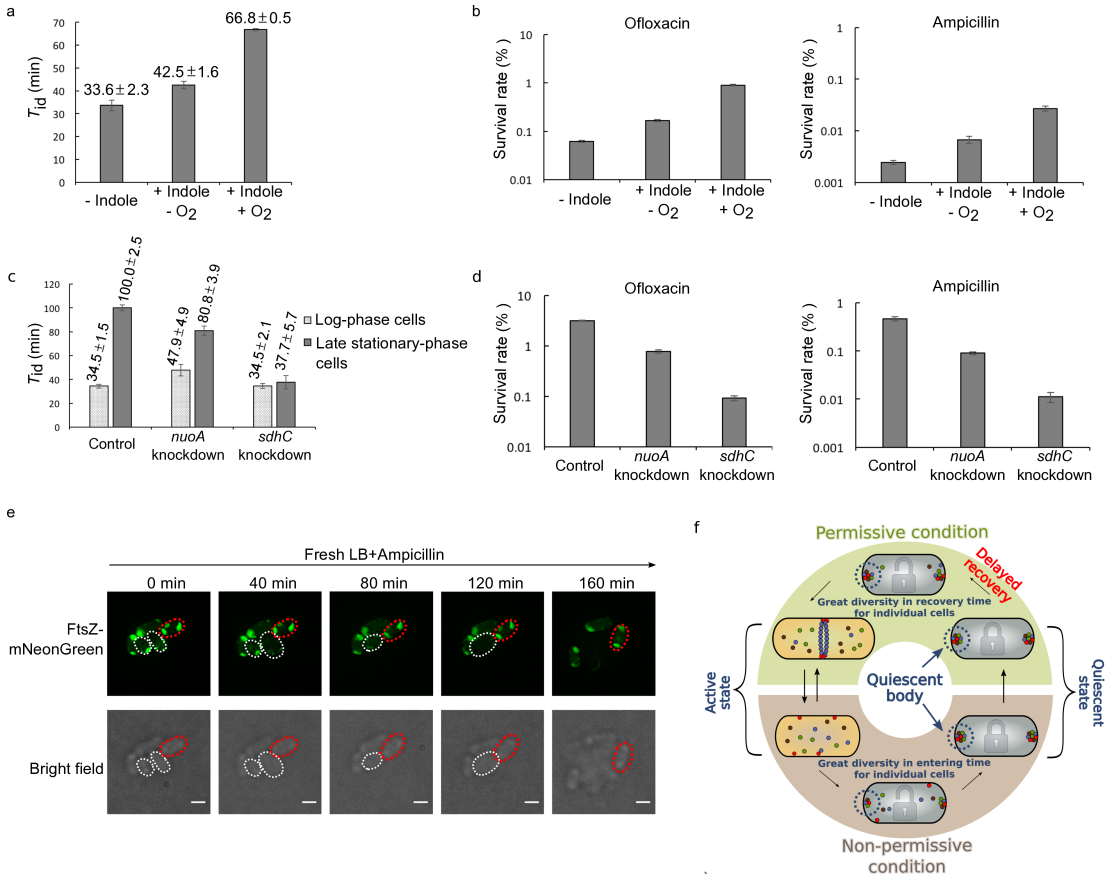

378

379 **Figure 5. Formation of cell pole granules delays the re-growth and re-division process and**
380 **thus endows the cells with a higher survival rate against antibiotic treatment.**
381 **(a)** The average initial doubling time upon re-division (T_{id}) of wild-type log-phase cells untreated
382 (- indole) or treated (+ indole) with indole (5 mM, 1 h) in the presence (+ O_2) or absence (- O_2) of
383 oxygen. The treated cells were re-cultured (diluted 40-fold) at 37℃ in fresh LB media. T_{id} was
384 calculated by measuring the increase in cell number within the first 45 min (for details, see
385 Methods). **(b)** Survival rates of wild-type log-phase cells that were treated with indole (+ indole)
386 in the presence (+ O_2) or absence (-O_2) of oxygen before re-culture in fresh LB media with the
387 addition of ofloxacin (5 μg/ml) or ampicillin (200 μg/ml). The survival rates were calculated as:
388 [colony-forming units of the antibiotic treated cells] / [colony-forming units of the untreated cells]
389 ×100. **(c)** The average initial doubling time upon re-division (T_{id}) of log-phase and late stationary-
390 phase cells with the knockdown of either the *nuoA* or the *sdhC* gene. The cells were re-cultured
391 (after 40-fold dilution) at 37℃ in fresh LB media. The T_{id} was calculated by measuring the
392 increase in cell number within the first 45 min (for details, see Methods). **(d)** Survival rates of the
393 late stationary-phase of either *nuoA* or *sdhC* knockdown cells re-cultured in fresh LB media
394 containing ofloxacin (5 μg/ml) or ampicillin (200 μg/ml). The survival rates were calculated as
395 in (**b**). At least three independent replicates were performed for each experimental condition. Each
396 data point is denoted by the mean value ± s.e. **(e)** Fluorescence and bright field images of the
397 late stationary-phase *ftsZ-mNeonGreen* cells that were re-cultured at 37℃ in fresh ampicillin-
398 containing LB media to the indicated time points. The re-growing and non-growing cells are

399 indicated by white and red dashed lines, respectively. Scale bars, 1 μm. **(f)** Schematic illustration
400 for the asynchronously reversible assembly of the cell pole granules in bacterial cells: The
401 formation of cell pole granules under non-permissive condition lock cells in quiescent states
402 resulting in failing to re-grow until the cell pole granules initiate to disassemble when permissive
403 conditions are restored.
404
405 **Discussion**
406
407 Here, we revealed a novel cytosolic organelle-like structure that is formed in non-
408 growing/non-dividing late stationary-phase *E. coli* cells but not in growing/dividing
409 log-phase *E. coli* cells. This structure is located at the cell poles, and its formation relies
410 on the normal operation of the respiratory chain. Formation of cell pole granules, into
411 which essential proteins for cell growth and division are locked, apparently marks a
412 quiescent state for the cells, which recover only when the cell pole granules are
413 disassembled to release those key sequestered components under permissive growth
414 conditions. We henceforth renamed the cell pole granule the "quiescent body", whose
415 reversible formation correlated with the quiescent state of bacterial cells is
416 schematically illustrated in **Fig. 5f**. Our model also reflects the finding that the great
417 diversity in the time taken for the quiescent bodies to disassemble underlies the great
418 diversity in the time taken for the quiescent bacterial cells to recover (commonly
419 defined as the delay time) under a permissive condition[16–18].
420 We speculate that for those so-called "viable but non-culturable" bacterial cells[34,35],
421 their quiescent bodies somehow remain in a non-disassembled state under the given
422 culture condition. With regard to the biological significance of this observed diversity
423 in quiescent body disassembly, it might be conjectured that under any particular
424 environmental condition, only part of the cells in the population will have their
425 quiescent bodies disassemble and thus reinitiate growth and division, while the rest of
426 the cells remain in a quiescent state. In this case, if the environmental condition still
427 proves to be non-permissive for cell growth/division, only the recovered cells will die.
428 Evidently, such diversity in quiescent body disassembly and cell recovery will provide
429 the best survival opportunity for the species in often highly unpredictable environments.
430 Alternatively, the heterogeneity that we observed for the quiescent bodies to
431 disassemble and cells to recover only reflected the different stages of the bacterial cells
432 in entering into an eventually homogeneous quiescent state ultimately. Future extensive
433 studies on the structure and function of the quiescent bodies, both under *in vitro*
434 conditions and in living cells, may help to resolve these issues.
435 It is likely that in addition to the key proteins that we identified in the quiescent
436 bodies, other types of biomolecules are also present, at least for maintaining a highly
437 compact structure. However, we detected no significant amount of glycogen based on
438 anthrone spectrophotometric analysis or amylase treatment[36] (data not shown). We also
439 did not detect a significant amount of DNA, mRNA, rRNA or tRNA. Despite these
440 findings, whether other polysaccharide molecules (such as peptidoglycan,

441 lipopolysaccharide) and nucleic acids are present in the quiescent body await future
442 investigation.
443 We have demonstrated that the formation of quiescent bodies relies on the active
444 operation of the cellular respiratory chain, but the detailed molecular mechanism behind
445 this observation awaits further exploration. It is believed that reactive oxygen species
446 (ROS), as represented by superoxide radical ($^{\cdot}O_2^-$) and hydroxyl free radical ($^{\cdot}OH$), are
447 byproducts of the respiratory chain. However, we detected no significant inducing
448 effect by adding H_2O_2, a type of ROS produced from superoxide radicals by the action
449 of superoxide dismutase[37], into the culture media for the formation of quiescent bodies
450 in log-phase cells. Nevertheless, this result could not rule out the possibility that other
451 ROS species serve as the factor that directly triggers the formation of quiescent bodies.
452 Quiescent body-containing cells exhibiting higher resistance to antibiotics (**Fig. 5b**
453 and **Fig. 5d**) are apparently similar or even identical to the clinically defined persister
454 cells, the most characteristic feature of which is high resistance to all antibiotics[38–40]. In
455 this regard, we noticed that the formation of persister cells in stationary-phase *E. coli*
456 cultures was reported to be associated with the formation of protein aggregates in the
457 cells[41,42]. Such aggregates, ill-defined as misfolded proteins by the authors, are very
458 likely to be identical to the quiescent bodies we revealed here. Furthermore, in support
459 of our present discovery, it was reported that the inhibition of cellular respiration in the
460 stationary phase would impair persister formation among *E. coli* cells[43]. In addition,
461 we suppose that the FtsZ puncta that were observed in *Mycobacterium tuberculosis* and
462 *Mycobacterium smegmatis*[44,45] also probably represent quiescent bodies. If this
463 assumption is proven to be true, it will indicate that quiescent body formation is a
464 conserved phenomenon, at least in bacteria. In light of these results, either blocking the
465 assembly or promoting the disassembly of quiescent bodies may reduce or block the
466 formation of persisters, thus greatly increasing the efficacy of antibiotics in killing
467 bacterial cells, especially towards those bacterial pathogens (e.g., *Mycobacterium*
468 *tuberculosis*) that easily enter the dormant state. Whether structures similar to the
469 quiescent bodies we describe here also exist in quiescent eukaryotic cells would
470 certainly be worth further investigation.

471

472 **METHODS**

473 **Bacterial strains, plasmids and genomic modifications.** The phenotypes of all the
474 bacterial strains used in this study, all derived from the *E. coli* BW25113 strain, are
475 listed in **Supplementary Table S1**. The plasmids used for fluorescence imaging and
476 CRISPRi experiments are listed in **Supplemental Table S2**. Genetic modifications of
477 the bacterial strains were performed using the λ–red genomic recombination system[46].
478 All the newly generated plasmids and genomic modifications were confirmed by DNA
479 sequencing.

480 **Chemicals, culture media and growth conditions.** Luria Bertani (LB) liquid (10 g/l
481 tryptone, 5 g/l yeast extract and 5 g/l NaCl) or agar-containing LB medium was
482 sterilized by autoclaving. For plasmid selection, 50 μg/ml kanamycin or 100 μg/ml
483 ampicillin was added to the culture medium. For the assay analyzing cell survival
484 against antibiotics, a final concentration of 5 μg/ml ofloxacin or 200 μg/ml ampicillin
485 was used. Log-phase and late stationary phase-cells respectively refer to cells that were
486 cultured for 6 h and 24 h at 37℃ in test tubes shaking at 260 r.p.m. After overnight
487 culture, the cells were diluted 100-fold into fresh LB media.

488 **Fluorescence microscopy.** Cell or cell lysate samples were dropped onto a glass dish
489 (NEST biotechnology) and covered with agar before micrographs were acquired at
490 37°C (for the re-growth experiments) or at 30°C (for all other experiments) on an N-
491 SIM imaging system (Nikon), with a 100X/1.49 NA oil-immersion objective (Nikon)
492 and after being excited by a 488 nm or 561 nm laser beam. The images were
493 reconstructed with NIS-Elements AR 4.20.00 (Nikon) software and further processed
494 with the GNU image manipulation program.

495 **Quiescent body isolation and immunoblotting analysis.** The bacterial cells were
496 grown at 37℃ by shaking at 260 r. p. m. for 24 h after overnight cultured cells were
497 diluted 100-fold into fresh LB medium. The cells were then collected by centrifugation
498 (8000 × g) and disrupted by a French press at 1000 MPa before centrifugation at 1,300
499 × g to collect the quiescent bodies in the pellet. Total cell lysate, the supernatant and
500 the pellet were each added into the sample buffer, boiled and analyzed by tricine SDS-
501 PAGE or further probed with the indicated antibodies for the immunoblotting analysis.
502 The visualized protein bands on the gels were scanned and processed using the GNU
503 image manipulation program.

504 **CRISPRi experiments.** These experiments were performed according to previously
505 reported methods[47]. Plasmids carrying the gRNA that targets the *nuoA* gene or *sdhC*
506 gene were transformed into the strain in which the proteins for recognizing and
507 binding specific DNA sequences are expressed and the gene encoding the protein to
508 cleave the target sequence is deleted. The designed sequences to knockdown the *nuoA*
509 gene and the *sdhC* gene were ATAGCGAATGCCCAGTGATGAGCGATGACTTC
510 and AATGTGAAAAAACAAAGACCTGTTAATCTGGA, respectively.

511 **Cell re-growth analysis and calculation of the average initial doubling time upon**
512 **re-division (T_{id}).** Log-phase or late stationary-phase cells of the indicated genotypes or
513 treatments were diluted 40-fold into fresh LB media and cultured at 37℃ with shaking
514 (260 r.p.m.). Growth curves were prepared by measuring the OD_{600} value of the
515 cultured cells at 45 min or 60 min intervals. The average initial doubling time upon re-
516 division (T_{id}) was calculated as 45/log (N_{t1}/N_{t0}, 2) min, where N_{t0} and N_{t1} represent the
517 number of cells at 0 min and 45 min, respectively. The N_{t1}/N_{t0} ratio for each batch of
518 cultured cells was calculated based on the increase in optical density at 600 nm (the

519 correlation between the cell number and the OD_{600} value was determined by preparing
520 a standard curve).

521 **Assay for cell survival against antibiotic treatment.** Late stationary-phase cells were
522 diluted 40-fold into fresh LB media containing either 5 μg/ml ofloxacin or 200 μg/ml
523 ampicillin and incubated at 37℃ with shaking (260 r.p.m.) for 2 h. The cells were then
524 centrifuged to remove the culture media and the antibiotics, re-suspended in phosphate-
525 buffered saline (PBS) and serially diluted in PBS before being spotted on LB agar plates
526 for colony formation unit counting. The cell survival rate was calculated as [number of
527 colonies formed after antibiotics treatment] / [number of colonies formed without
528 antibiotics treatment] ×100.

529 **Acknowledgments**
530 We thank Keio Collections for providing the wild-type and Δ*tnaA* strains. We
531 thank the Core Facilities at School of Life Sciences, Peking University, for assistance
532 with SIM, and we are grateful to Chunyan Shan and Xiaochen Li for their help with
533 fluorescence imaging. We thank Dr. Wen Zhou at the Mass Spectrometry Facility of
534 the National Center for Protein Sciences at Peking University for assistance in
535 performing the mass spectrometry analysis. We thank Prof. Xinmiao Fu from Fujian
536 Normal University for useful discussions. This work was supported by funds from the
537 National Natural Science Foundation of China (No. 31670775 and 31470766 to ZYC)
538 and the National Basic Research Program of China (No. 2012CB917300 to ZYC).

539 **Author Contributions**
540 Jiayu Yu and Yang Liu designed and performed the experiments, analyzed the data
541 and drafted the manuscript. Prof. Zengyi Chang edited the manuscript and supervised
542 this study.

543 **Conflict of Interest**
544 We declare that we have no conflicts of interest related to this work.

545

546 **References**

547 1. Lutkenhaus, J., Pichoff, S. & Du, S. Bacterial cytokinesis: From Z ring to
548 divisome. *Cytoskeleton* **69,** 778–790 (2012).
549 2. Natale, P., Pazos, M. & Vicente, M. The *Escherichia coli* divisome: born to
550 divide: Cell division in *Escherichia coli*. *Environ. Microbiol.* **15,** 3169–3182
551 (2013).

552 3. Rowlett, V. W. & Margolin, W. The bacterial divisome: ready for its close-up.
553 *Philos. Trans. R. Soc. B Biol. Sci.* **370,** 20150028 (2015).
554 4. Bi, E. F. & Lutkenhaus, J. FtsZ ring structure associated with division in
555 Escherichia coli. *Nature* **354,** 161–164 (1991).
556 5. Adams, D. W. & Errington, J. Bacterial cell division: assembly, maintenance and
557 disassembly of the Z ring. *Nat. Rev. Microbiol.* **7,** 642–653 (2009).
558 6. Sun, Q. & Margolin, W. FtsZ dynamics during the division cycle of live
559 Escherichia coli cells. *J. Bacteriol.* **180,** 2050–2056 (1998).
560 7. Scheffers, D. & Driessen, A. J. The polymerization mechanism of the bacterial
561 cell division protein FtsZ. *FEBS Lett.* **506,** 6–10 (2001).
562 8. Mingorance, J., Rivas, G., Vélez, M., Gómez-Puertas, P. & Vicente, M. Strong
563 FtsZ is with the force: mechanisms to constrict bacteria. *Trends Microbiol.* **18,**
564 348–356 (2010).
565 9. Chin, J. W., Martin, A. B., King, D. S., Wang, L. & Schultz, P. G. Addition of a
566 photocrosslinking amino acid to the genetic code of Escherichiacoli. *Proc. Natl.*
567 *Acad. Sci. U. S. A.* **99,** 11020–11024 (2002).
568 10. Ryu, Y. & Schultz, P. G. Efficient incorporation of unnatural amino acids into
569 proteins in Escherichia coli. *Nat. Methods* **3,** 263–265 (2006).
570 11. Zhang, M. *et al.* A genetically incorporated crosslinker reveals chaperone
571 cooperation in acid resistance. *Nat. Chem. Biol.* **7,** 671–677 (2011).

572 12. Wang, Y. *et al.* A Supercomplex Spanning the Inner and Outer Membranes
573 Mediates the Biogenesis of β-Barrel Outer Membrane Proteins in Bacteria. *J.*
574 *Biol. Chem.* **291,** 16720–16729 (2016).
575 13. Fu, X., Shi, X., Yan, L., Zhang, H. & Chang, Z. In Vivo Substrate Diversity and
576 Preference of Small Heat Shock Protein IbpB as Revealed by Using a Genetically
577 Incorporated Photo-cross-linker. *J. Biol. Chem.* **288,** 31646–31654 (2013).
578 14. Sezonov, G., Joseleau-Petit, D. & D'Ari, R. Escherichia coli Physiology in Luria-
579 Bertani Broth. *J. Bacteriol.* **189,** 8746–8749 (2007).
580 15. Ma, X., Ehrhardt, D. W. & Margolin, W. Colocalization of cell division proteins
581 FtsZ and FtsA to cytoskeletal structures in living Escherichia coli cells by using
582 green fluorescent protein. *Proc. Natl. Acad. Sci. U. S. A.* **93,** 12998–13003 (1996).
583 16. Sezonov, G., Joseleau-Petit, D. & D'Ari, R. Escherichia coli Physiology in Luria-
584 Bertani Broth. *J. Bacteriol.* **189,** 8746–8749 (2007).
585 17. Novick, A. Growth of Bacteria. *Annu. Rev. Microbiol.* **9,** 97–110 (1955).
586 18. Penfold, W. J. On the Nature of Bacterial Lag. *J. Hyg. (Lond.)* **14,** 215–241
587 (1914).
588 19. Carrio, M. M. & Villaverde, A. Localization of Chaperones DnaK and GroEL in
589 Bacterial Inclusion Bodies. *J. Bacteriol.* **187,** 3599–3601 (2005).
590 20. Weiner, J. H. & Li, L. Proteome of the Escherichia coli envelope and
591 technological challenges in membrane proteome analysis. *Biochim. Biophys. Acta*
592 *BBA - Biomembr.* **1778,** 1698–1713 (2008).

593 21. Wolfe, A. D. & Hahn, F. E. Mode of action of chloramphenicol IX. Effects of
594 chloramphenicol upon a ribosomal amino acid polymerization system and its
595 binding to bacterial ribosome. *Biochim. Biophys. Acta BBA - Nucleic Acids*
596 *Protein Synth.* **95,** 146–155 (1965).
597 22. Durand-Heredia, J. M., Yu, H. H., De Carlo, S., Lesser, C. F. & Janakiraman, A.
598 Identification and Characterization of ZapC, a Stabilizer of the FtsZ Ring in
599 Escherichia coli. *J. Bacteriol.* **193,** 1405–1413 (2011).
600 23. Ghigo, J. M. & Beckwith, J. Cell division in Escherichia coli: role of FtsL
601 domains in septal localization, function, and oligomerization. *J. Bacteriol.* **182,**
602 116–129 (2000).
603 24. Wolfe, A. J. The Acetate Switch. *Microbiol. Mol. Biol. Rev.* **69,** 12–50 (2005).
604 25. Lee, J.-H. & Lee, J. Indole as an intercellular signal in microbial communities.
605 *FEMS Microbiol. Rev.* **34,** 426–444 (2010).
606 26. Gaimster, H. & Summers, D. Regulation of Indole Signalling during the
607 Transition of E. coli from Exponential to Stationary Phase. *PLOS ONE* **10,**
608 e0136691 (2015).
609 27. Newton, W. A. & Snell, E. E. FORMATION AND INTERRELATIONSHIPS OF
610 TRYPTOPHANASE AND TRYPTOPHAN SYNTHETASES IN
611 ESCHERICHIA COLI. *J. Bacteriol.* **89,** 355–364 (1965).

612 28. Chimerel, C., Murray, A. J., Oldewurtel, E. R., Summers, D. K. & Keyser, U. F.
613 The Effect of Bacterial Signal Indole on the Electrical Properties of Lipid
614 Membranes. *ChemPhysChem* **14,** 417–423 (2013).
615 29. Basan, M. *et al.* Overflow metabolism in Escherichia coli results from efficient
616 proteome allocation. *Nature* **528,** 99–104 (2015).
617 30. Luo, M. L., Mullis, A. S., Leenay, R. T. & Beisel, C. L. Repurposing endogenous
618 type I CRISPR-Cas systems for programmable gene repression. *Nucleic Acids*
619 *Res.* **43,** 674–681 (2015).
620 31. Lewis, K. Persister cells, dormancy and infectious disease. *Nat. Rev. Microbiol.* **5,**
621 48–56 (2007).
622 32. Völzing, K. G. & Brynildsen, M. P. Stationary-Phase Persisters to Ofloxacin
623 Sustain DNA Damage and Require Repair Systems Only during Recovery. *mBio*
624 **6,** e00731-715 (2015).
625 33. Fridman, O., Goldberg, A., Ronin, I., Shoresh, N. & Balaban, N. Q. Optimization
626 of lag time underlies antibiotic tolerance in evolved bacterial populations. *Nature*
627 **513,** 418–421 (2014).
628 34. Xu, H. S. *et al.* Survival and viability of nonculturableEscherichia coli andVibrio
629 cholerae in the estuarine and marine environment. *Microb. Ecol.* **8,** 313–323
630 (1982).

631 35. Li, L., Mendis, N., Trigui, H., Oliver, J. D. & Faucher, S. P. The importance of
632 the viable but non-culturable state in human bacterial pathogens. *Front.*
633 *Microbiol.* **5,** 258 (2014).
634 36. Makinoshima, H. *et al.* Growth Phase-Coupled Alterations in Cell Structure and
635 Function of Escherichia coli. *J. Bacteriol.* **185,** 1338–1345 (2003).
636 37. Korshunov, S. & Imlay, J. A. Two sources of endogenous hydrogen peroxide in
637 *Escherichia coli*. *Mol. Microbiol.* **75,** 1389–1401 (2010).
638 38. Allison, K. R., Brynildsen, M. P. & Collins, J. J. Heterogeneous bacterial
639 persisters and engineering approaches to eliminate them. *Curr. Opin. Microbiol.*
640 **14,** 593–598 (2011).
641 39. Allison, K. R., Brynildsen, M. P. & Collins, J. J. Metabolite-enabled eradication
642 of bacterial persisters by aminoglycosides. *Nature* **473,** 216–220 (2011).
643 40. Amato, S. M. & Brynildsen, M. P. Persister Heterogeneity Arising from a Single
644 Metabolic Stress. *Curr. Biol. CB* **25,** 2090–2098 (2015).
645 41. Kwiatkowska, J., Matuszewska, E., Kuczyńska-Wiśnik, D. & Laskowska, E.
646 Aggregation of Escherichia coli proteins during stationary phase depends on
647 glucose and oxygen availability. *Res. Microbiol.* **159,** 651–657 (2008).
648 42. Leszczynska, D., Matuszewska, E., Kuczynska-Wisnik, D., Furmanek-Blaszk, B.
649 & Laskowska, E. The Formation of Persister Cells in Stationary-Phase Cultures of
650 Escherichia Coli Is Associated with the Aggregation of Endogenous Proteins.
651 *PLoS ONE* **8,** e54737 (2013).

652 43. Orman, M. A. & Brynildsen, M. P. Inhibition of stationary phase respiration
653 impairs persister formation in E. coli. *Nat. Commun.* **6,** 7983 (2015).
654 44. Chauhan, A. *et al.* Mycobacterium tuberculosis Cells Growing in Macrophages
655 Are Filamentous and Deficient in FtsZ Rings. *J. Bacteriol.* **188,** 1856–1865
656 (2006).
657 45. Dziedzic, R. *et al.* Mycobacterium tuberculosis ClpX Interacts with FtsZ and
658 Interferes with FtsZ Assembly. *PLoS ONE* **5,** e11058 (2010).
659 46. Lee, D. J. *et al.* Gene doctoring: a method for recombineering in laboratory and
660 pathogenic Escherichia coli strains. *BMC Microbiol.* **9,** 252 (2009).
661 47. Luo, M. L., Mullis, A. S., Leenay, R. T. & Beisel, C. L. Repurposing endogenous
662 type I CRISPR-Cas systems for programmable gene repression. *Nucleic Acids*
663 *Res.* **43,** 674–681 (2015).